# Synthesis of $MoS_2$ Inorganic Fullerene-like Nanoparticles by a Chemical Vapour Deposition Method

**Bin Gao* and Xiaojun Zhang**

*School of Science, Xi'an Polytechnic University, Xi'an 710048, China.*

Received 31 December 2012, revised 6 September 2013, accepted 13 September 2013.

ABSTRACT

**$MoS_2$ nanoparticles with fullerene-like structure (*IF*-$MoS_2$) were successfully obtained at heating temperature higher than 840 °C by a chemical vapour deposition method using $MoO_3$ and sulfur powders as raw materials. The synthesized samples were characterized by XRD, SEM, TEM, EDX and Raman spectrometry, respectively. The reaction temperature has important influences on composition and morphology of the products, and pure *IF*-$MoS_2$ nanoparticles can be obtained only in the narrow temperature range of 840–870 °C. Diffraction peak (002) of *IF*-$MoS_2$ nanoparticles moves to small angle compared to that of 2H-$MoS_2$, indicating that the adjacent lattice spacing along the c-axis of *IF*-$MoS_2$ nanoparticles is about 2 % larger than that of layered 2H-$MoS_2$. The peaks at 155 $cm^{-1}$, 349.8 $cm^{-1}$ and 281.7 $cm^{-1}$ in the Raman spectrum of bulk and layered $MoS_2$ are absent, which is attributed to $MoS_2$ layer folding or curling along Γ-M in Brillouin zone to form fullerene-like polyhedra and nanotubes. In addition, a gradual formation mechanism of *IF*-$MoS_2$ nanoparticles was discussed in detail.**

KEYWORDS

**Synthesis, molybdenum disulfide, nanoparticles, fullerene-like structure, chemical vapour deposition.**

## 1. Introduction

The discovery of carbon fullerenes and nanotubes,[1,2] their outstanding properties and potential applications, has attracted intense experimental and theoretical interest. The propensity of graphite nanoparticles to form hollow closed structures stems from the high energy of dangling bonds at the periphery of the nanoparticles, and the property is also common to layered transition metal chalcogenides including sulfides, selenides and tellurides.[3–6] The layered semiconductor molybdenum disulfide ($MoS_2$), composed of S-Mo-S trilayers and separated by relatively large Van der Waals gap, present many interesting characteristics in several fields, such as catalysis, photoconductivity, hydrosulfurization and triboloical properties.[7] Applications of pure $MoS_2$ powder could be envisioned in high vacuum and microelectronics equipment, where organic residues with high vapour pressure can lead to severe contamination problems. Unfortunately, $MoS_2$ platelets tend to adhere to the metal surfaces through their reactive prismatic edges, in which configuration they 'glue' the two metal surfaces together rather than serve as a solid lubricant. During the mechanical action of the engine parts, abrasion and burnishing of the solid lubricant produce smaller and smaller platelets and increase their surface area and, consequently, they tend to stick to the metal surfaces through their reactive prismative edges. The exposed prismatic edges are reactive sites, which facilitate chemical oxidation of the platelets. These phenomena adversely affect the tribological benefits of the solid lubricant. The spherical shape of inorganic fullerene-like $MoS_2$ (*IF*-$MoS_2$) nanoparticles and their inert sulfur-terminated surface suggest that *IF*-$MoS_2$ nanoparticles can be used as a solid lubricant additive in lubrication fluids, greases and even in solid matrices. *IF*-$MoS_2$ nanoparticles are expected to behave like nano-ball bearings and upon mechanical stress they would slowly exfoliate or mechanically deform to the shape of a rugby ball, but would not lose their tribological benefit, until they are completely gone, or oxidized.[8–10] Apart from the outstanding mechanical properties,[11,12] inorganic fullerene-like $MoS_2$ nanoparticles and nanotubes have drawn a great deal of attention for their interesting properties and important applications as solid-state secondary lithium battery cathodes,[13] hydrogen storage,[14] host-guest compounds,[15] scanning tunnelling microscope tip[16] and industrial catalysts for hydrodesulfurization of crude oil.[17]

Quite a few techniques for the synthesis of large amounts of inorganic fullerene-like $MoS_2$ nanoparticles and nanotubes,[18–21] which were first reported by R.Tenne *et al.*,[3] have been developed. For example, R. Tenne and co-workers reported the production of *IF*-$MoS_2$ by the gas phase reaction between $MoO_3$ and $H_2S$ in a reducing atmosphere (5 % $H_2$ + 95 % $N_2$) at high temperature,[4] Chen *et al.* synthesized $MoS_2$ nanotubes by direct reaction of $(NH_4)_2MoS_4$ and hydrogen at a relatively low temperature about 400 °C,[14,17] Hsu *et al.* described the generation of $MoS_2$ nanotubes with well-defined tube walls and free of encapsulated material by heating $MoS_2$ powder covered by Mo foil to *ca.* 1300 °C in the presence of $H_2S$,[22] and closed caged fullerene-like molybdenum disulfide nanoparticles were obtained *via* an arc discharge between a graphite cathode and a molybdenum anode filled with microscopic $MoS_2$ powder submerged in deionized water.[23] However, developing new synthetic strategies and further understanding of the formation mechanism of fullerene-like $MoS_2$ nanoparticles and nanotubes are still challenges for scientists. In this article, we report an alternative cost-effective method for synthesis of *IF*-$MoS_2$ nanoparticles. The method exploits a simple apparatus that does not require toxic gas $H_2S$, vacuum equipment or costly lasers, and may offer an opportunity for further investigation on $MoS_2$, and will serve as a general route to the formation of transitional metal dichalcogenides.

## 2. Experimental

Synthesis of inorganic fullerene-like $MoS_2$ nanoparticles was carried out in a horizontal gas-phase reactor lying in a

* To whom correspondence should be addressed. E-mail: gaobin7401@sina.com

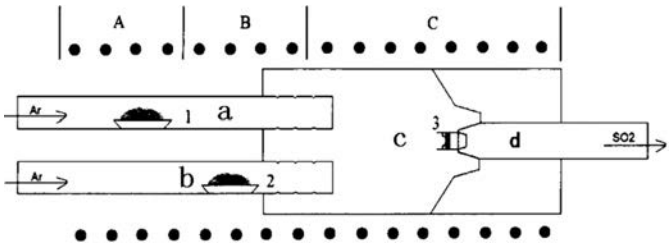


**Figure 1** Schematic representation of the experimental horizontal gas-phase reactor: tube *a*, *b* served for sublimation of sulfur and $MoO_3$ powder in an inert atmosphere Ar; tube *c* served for gas-phase reaction chamber of sulfur and $MoO_3$ vapours; tube *d* with a ceramic filter in the forepart, served for gas exit.

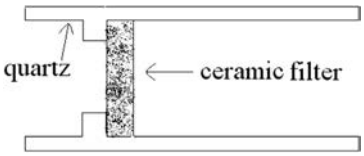


**Figure 2** Schematic representation of the ceramic filter in the forepart of tube *d*.

three-zone tube furnace. The reactor, consisting of four quartz tubes, is depicted in Fig. 1. Tubes *a* and *b* served for sublimation of S (sulfur) and $MoO_3$ powders in the argon (Ar) atmosphere. S and $MoO_3$ powders were placed in two small quartz boats (boats 1 and 2) inside tubes *a* and *b*, respectively. The heated S and $MoO_3$ powders were sublimed and swept by the Ar stream into the tube *c* through several pinholes in tubes *a* and *b* (see Fig. 1), in which the reaction took place. Tube *d* was used for gas exit. The reaction products were collected on a ceramic filter in the forepart of tube *d* (as shown in Fig. 2).

Typical experimental procedures were as follows: quartz boats 1 and 2 with S (22.4 g) and $MoO_3$ (2.9 g) powders were positioned in zone A and B of a three-zone tube furnace, respectively. Highly pure argon gas (>99.999 %) was passed through the tubes in order to remove atmosphere and steam in the reactor, then a gas flow meter was adjusted to the required argon flow rate when zone C was heated to 550 °C with heating rate 10 °C $min^{-1}$; finally the temperatures of zones A, B and C reached and were maintained at 420 °C, 650 °C and 840 °C, respectively, for 120 min. The reactor was cooled to room temperature in argon atmosphere and then black $MoS_2$ powders were collected on a ceramic filter for analysis.

Structural characterization of products was analyzed by an X-ray powder diffractometer (XRD; RIGAKU D/max-2400, Tokyo, Japan) with Cu k$\alpha$ radiation ($\lambda = 0.15418$ nm) at 40 kV, 200 mA. The morphology, structure and composition of the samples were determined using a scanning electron microscopy (SEM; S-3400N, Hitachi, Tokyo, Japan) and transmission electron microscopy (TEM; JEM-3010, JEOL, Tokyo, Japan) equipped with an energy dispersive X-ray spectrometer (EDX, S-570, Japan) and operated at 200 keV. Raman spectra were taken under ambient conditions using a Renishaw in a Via Raman microscope spectrometer (System-1000, Renishaw, Woburn, MA, USA) excited with a 632.8 nm $Ar^+$ laser.

## 3. Results and Discussion

In order to obtain pure *IF*-$MoS_2$ nanoparticles, $MoS_2$ powders were synthesized by $MoO_3$ and S at various reaction temperatures (zone C of tube furnace in Fig. 1). Figure 3 presents the XRD patterns of the products synthesized at 650 °C, 700 °C, 750 °C, respectively, keeping the high pure argon flow rate constant. In addition to $MoS_2$ peaks, the XRD patterns of products include peaks from $MoO_3$ and $MoO_2$ at 650 °C, and $MoO_2$ peaks at 700 °C. Impure products are obtained at both temperatures, comprising $MoS_2$, $MoO_3$ and $MoO_2$ at 650 °C and $MoS_2$ and $MoO_2$at 700 °C. It shows that the reaction does not take place completely, leading to presence of reaction intermediate ($MoO_2$) and raw material ($MoO_3$). No impurity peaks were observed from the XRD spectrum of the products synthesized at 750 °C. All the peaks can be indexed to $MoS_2$, which is in good agreement with the reported value from standard card (JCPDS No. 77-1716). The XRD patterns indicate that very pure $MoS_2$ powders were synthesized at 750 °C. Although reaction of $MoO_3$ and S can occur to form $MoS_2$ at 600 °C,[24] it takes a long reaction time to generate $MoS_2$ by the reaction between $MoO_3$ and S gas molecules with low activity at 650 °C, 700 °C. Therefore, the products are not pure $MoS_2$ at lower temperatures (<750 °C). The activity of $MoO_3$ and S sublimations increases with reaction temperature, leading to the generation of pure $MoS_2$ during short time and becoming conformation.

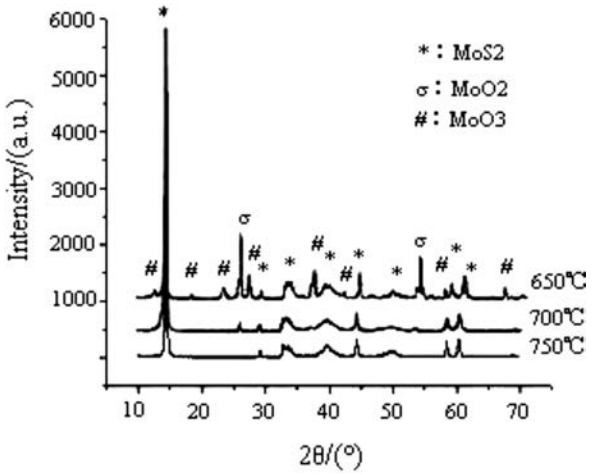


**Figure 3** XRD patterns of the as-synthesized $MoS_2$ products at different reaction temperatures.

Figure 4 shows a series of SEM images of $MoS_2$ powders synthesized at 800 °C, 840 °C, 870 °C, 900 °C, respectively, keeping the argon flow rate constant. It can be seen that $MoS_2$ crystals with platelet structure obtained at 800 °C, whose shapes were principally quasi-round or regular hexagon, are uniform and loose nanoparticles with size about 150–300 nm (Fig. 4a). At 840 °C, $MoS_2$ nanoparticles with quasi-sphere structure are synthesized, with sphere diameter of approximately 60–90 nm (Fig. 4b). $MoS_2$ nanoparticles with quasi-sphere structure were observed as well at 870 °C (Fig. 4c), with diameter about 200 nm, which is greater than that of products obtained at 840 °C. At 900 °C, reaction products are $MoS_2$ nanoparticles with similar shape to that synthesized at 800 °C, the diameters of the nanoparticles are larger than that of samples synthesized below 900 °C. Meanwhile, a $MoS_2$ micrometer particle, with diameter around 2000 nm, was observed (arrow in Fig. 4d), it might be formed of $MoS_2$ nanosheets interconnecting. The experimental results above demonstrate that the diameters of $MoS_2$ nanoparticles with same structure (platelet or sphere) may increase with reaction temperature.

Figure 5a is a HRTEM image of a randomly chosen single *IF*-$MoS_2$ nanoparticle synthesized at 840 °C from $MoO_3$ and S powders. The diameter of the *IF*-$MoS_2$ nanoparticle is about 60 nm, and the crystal lattice is similar to structure of fullerene $C_{60}$, consisting of a series of empty spheres with different diameters. Figure 5b presents a TEM image of an optional individual $MoS_2$

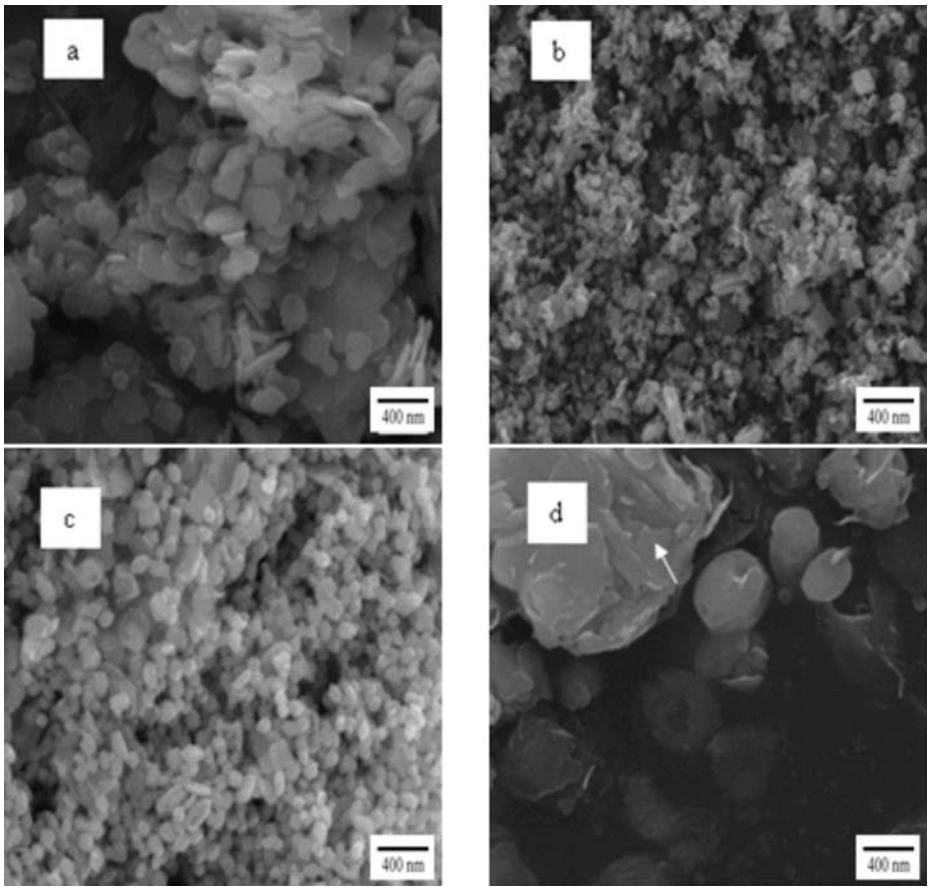


**Figure 4** SEM images of the as-synthesized $MoS_2$ samples at different temperatures. (**a**) 800 °C; (**b**) 840 °C; (**c**) 870 °C; (**d**) 900 °C.

nanoparticle obtained at 870 °C. Because of the diameter of the nanoparticle being too large (about 220 nm), the entire lattice structure of the *IF*-$MoS_2$ nanoparticles is hardly displayed. The fringe structure of the marginal part (the box diagram at the bottom left corner in Fig. 5b) of the *IF*-$MoS_2$ nanoparticle is displayed in Fig. 5c (the inset HRTEM image at the top right corner in Fig. 5b).We can see that $MoS_2$ layers terminate and layers dislocate (black arrow in Fig. 5a and Fig. 5c); generally, it is attributed to the formation of defects of the $MoO_3$ precursor nanoparticles or the short-term shortage of supply of raw materials in *IF*-$MoS_2$ nanoparticles formation process.[4,25] Simultaneously, crystal lattice fringe of $MoS_2$ nanoparticles with fullerene-like (*IF*-$MoS_2$) is 0.632 nm (the distance between white arrows in Fig. 5c), which is larger than the value of 2H-$MoS_2$ (0.612 nm). The lattice expansion is about 3.2 %, which is attributed to the less strain in the bent $MoS_2$ layers. Energy dispersive X-ray (EDX) spectrum measurement was used to characterize the overall chemical composition of the *IF*-$MoS_2$ nanoparticle, and the result is shown in Fig. 6. Strong peaks associated with S and Mo are found in the spectrum. The Cu signal comes from copper grid used to support sample in the process of TEM analysis. Quantitative analysis shows that Mo: S is about 1:2.02, consistent with atomic ratio of $MoS_2$ structure, which proves that the synthesized products are *IF*-$MoS_2$ nanoparticles.

*IF*-$MoS_2$ nanoparticles are generated by sulfidization of suboxide $MoO_{3-x}$ nanoparticles,[4] which are products of partial

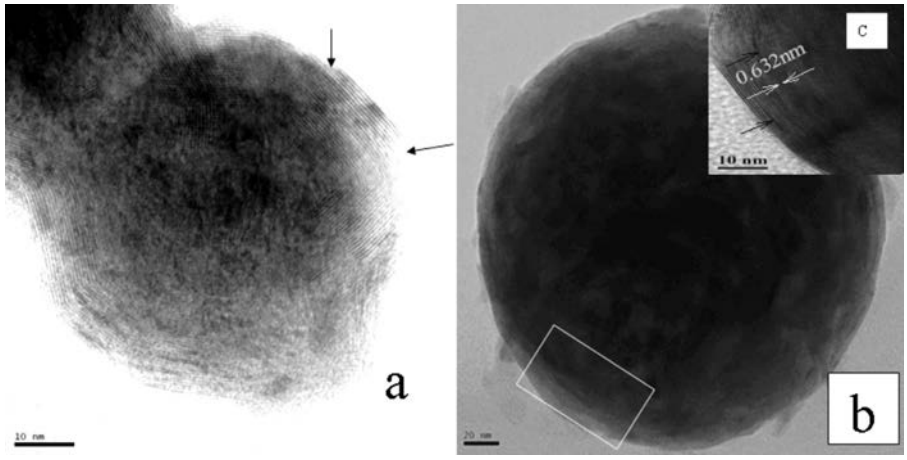


**Figure 5** Representative TEM images of the as-synthesized *IF*-$MoS_2$ products: (**a**) HRTEM image of an individual fullerene-like $MoS_2$ nanoparticle as-synthesized at 840 °C and (**b**) at 870 °C; (**c**) HRTEM image of an edge of the fullerene-like $MoS_2$ nanoparticle in (**b**) – the distance between two crystal fringes is 0.632 nm.

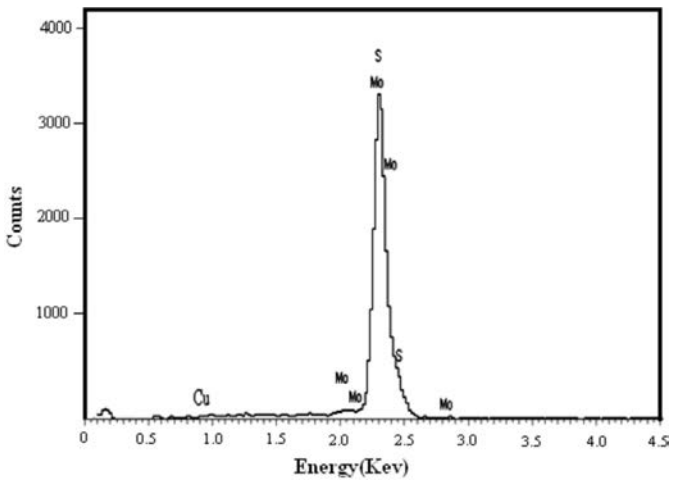


**Figure 6** EDX spectrum of the fullerene-like $MoS_2$ the as-synthesized nanoparticles, The Cu peak comes from copper grid used to support sample in process of TEM analysis.

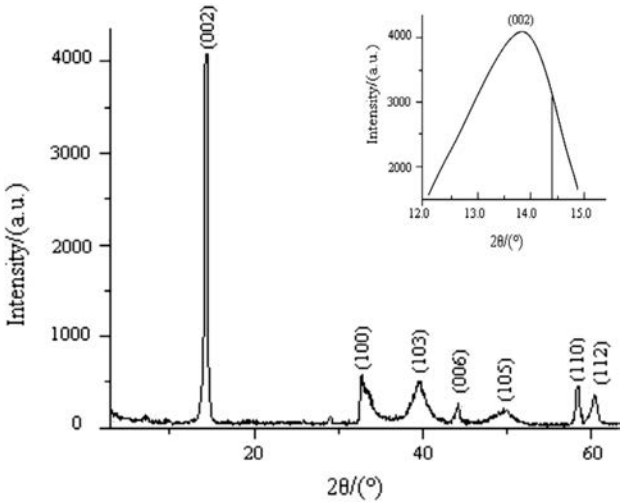


**Figure 7** XRD patterns of the synthesized *IF*-$MoS_2$ powders at 870 °C; the inset at top right corner is of an enlarged pattern of the (002) peak with a shift to a lower angle as compared to that of hexagonal 2H-$MoS_2$ crystal.

reduction of the molybdenum trioxide molecular clusters. According to the model, a synergy between the reduction and the sulfidization processes which occurs in a very narrow window of parameters is necessary, if not, the 2H-$MoS_2$ would form.[25–27] Reaction temperature plays an important role in synthesizing fullerene-like $MoS_2$ (*IF*-$MoS_2$) nanoparticles. The precursor $MoO_3$ molecular cluster is composed of two octahedra connected *via* a corner oxygen atom. While $MoO_3$ molecular clusters are reduced into $MoO_{3-x}$ nanoparticles, a few oxygen atoms leave the octahedron, and oxygen vacancies are thus formed. Lower critical concentration (threshold value) of vacancy is required for the shear process to occur at higher temperature. The induction period for generation of threshold concentration of vacancy on the crystallite surface decreases with temperature. At lower temperatures (800 °C), the rate of the shear process (reduction) is slow compared with sulfuring by the vacancy and consequently sulfur trapping predominates. At higher temperatures (900 °C), the rates of both the shear process and sulfur trapping increase with temperature, the former one predominates. At intermediate temperatures (840–870 °C), the rates of both processes have the same order of magnitude and, moreover, sulfidization and shear appear at the same time, leading to the formation of inorganic fullerene-like $MoS_2$.

The experimental results show that diameters of *IF*-$MoS_2$ nanoparticles increase with reaction temperature. $MoS_2$ layer formed in the process of partial reduction of $MoO_3$ nanoparticles is chemically inert and prevented $MoO_3$ nanoparticles from growing further, therefore the *IF*-$MoS_2$ nanoparticles diameters are determined by that of precursor $MoO_3$ nanoparticles.[28] The vapour phase of $MoO_3$ consists predominantly of the molecular clusters $Mo_3O_9$, $Mo_4O_{12}$ and $Mo_5O_{15}$.[29] The cluster $Mo_3O_9$, which has a hexagonal ring structure, is the most stable one, and consequently, it is the most volatile cluster of the three. In the next step, these clusters condense into $MoO_3$ nanoparticles. At a lower temperature, volatilization of $MoO_3$ powder is slower, $(MoO_3)_3$ molecular clusters concentration in tube *b* is lower. Due to smaller collision probability of the molecular clusters, the diameters of precursor $MoO_3$ nanoparticles condensed by these clusters are minor. Thus, finally obtained *IF*-$MoS_2$ nanoparticles are smaller. On the contrary, with increasing reaction temperature, $MoO_3$ powder volatilizes quickly, the diameters of $MoO_3$ nanoparticles are accreted, leading to the formation of bigger *IF*-$MoS_2$ nanoparticles. The diameter of $MoO_3$ nanoparticles precursor converting into *IF*-$MoS_2$ nanoparticles, however, has a critical value about 300 nm reported by R. Tenne and co-workers.[30] Above that value, 2H-$MoS_2$ platelets will be obtained. Therefore, reaction temperature at and above 900 °C the diameters of $MoO_3$ precursor nanoparticles are larger than 300 nm and 2H-$MoS_2$ platelets are synthesized finally. The size of the layered $MoS_2$ nanoparticles obtained at low temperature (800 °C) is larger than that of *IF*-$MoS_2$ nanoparticles at high temperature (840 °C and 870 °C), which is due to predomination of sulfur trapping at this time.

Figure 7 presents the XRD pattern of the *IF*-$MoS_2$ powder synthesized at 870 °C. We can see that all the diffraction peaks in the XRD spectrum of the sample can be indexed to $MoS_2$, which indicates that the product is pure *IF*-$MoS_2$. The inset at top right corner is an enlarged pattern of the (002) peak of XRD spectrum of the *IF*-$MoS_2$ powder with diffraction angle of 12–15 °. The inset pattern displays that (002) peak of *IF*-$MoS_2$ lies in 13.89 °, that of layered hexagonal 2H-$MoS_2$ is at >14.38 ° (vertical line as shown in the inset pattern),which shows that the position of the (002) peak of *IF*-$MoS_2$ shifts to a lower angle. The shift indicates a lattice expansion of *ca.* 3.2 % between two adjacent $MoS_2$ slabs along c-axis, the value is consistent with HRTEM result and larger than that *(ca.* 2 %) reported in literature.[4] It is generally considered that this shift is attributed to the less strain in the bent layers. Furthermore, since the number of atoms in the layers increases with nanoparticles radius, the layers cannot be fully commensurate.[26] According to the literature,[4,25,26] the shift proves that $MoS_2$ has a fullerene-like structure. The result is in accordance with the conclusions of the HRTEM observation.

Raman spectrum measured at room temperature of *IF*-$MoS_2$ powder obtained at 870 °C is shown in Fig. 8, the excitation source used for the argon ion laser with wavelength 632.8 nm. Raman spectrum is the same as those obtained by G.L. Frey,[30] and all characteristic peaks are less than 833 $cm^{-1}$. Two strongest characteristic peaks of synthesized *IF*-$MoS_2$, at 375.7 $cm^{-1}$ and 402.2 $cm^{-1}$, are at lower wave numbers than those (378 $cm^{-1}$ and 407 $cm^{-1}$) of samples synthesized by G.L. Frey. They are at 384 $cm^{-1}$ and 409 $cm^{-1}$ in 2H-$MoS_2$ spectrum, which correspond to $E_{2g}$ and $A_{1g}$ vibration modes respectively.[31] The peaks of 155.1 $cm^{-1}$, 349.8 $cm^{-1}$, 281.7 $cm^{-1}$ are absent in bulk and layered 2H-$MoS_2$.[31] Raman spectrum of *IF*-$MoS_2$ obtained by G.L. Frey only exist 283 $cm^{-1}$ peak, and simultaneously exist 155 $cm^{-1}$ peak by L.D. Whitby,[26] which are attributed to $MoS_2$ layers folding or

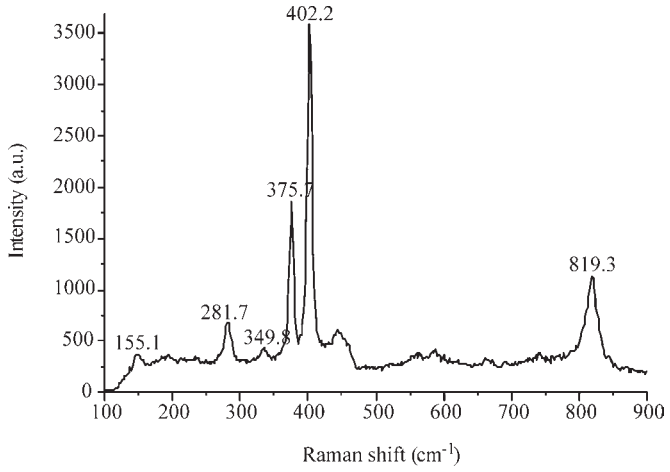


**Figure 8** Raman spectrum of synthesized fullerene-like $MoS_2$ powder.

curling along Γ-M direction of Brillouin zone to form fullerene-like polyhedron and nanotube.[26] This is strong evidence that $MoS_2$ samples obtained in our experiments have inorganic fullerene-like structure. All wave numbers of characteristic peaks of the samples are lower than that reported previously, that may be attributed to differences in experimental conditions.

R. Tenne and co-workers think fullerene-like $MoS_2$ nanoparticles and nanotubes are formed by reacting the $MoO_3$ vapour with $H_2S$ in the reduction atmosphere (5 % $H_2$ + 95 % $N_2$) step by step, reaction equations can be described by[4,24,25]

$$MoO_3 + x\ H_2 \rightarrow MoO_{3-x} + x\ H_2O \quad (1)$$

$$MoO_{3-x} + (1 - x)\ H_2 + 2H_2S \rightarrow MoS_2 + (3 - x)\ H_2O \quad (2)$$

In our approach, large amounts of fullerene-like $MoS_2$ nanoparticles were synthesized through reaction of $MoO_3$ precursors with sulfur vapour, in which S, instead of $H_2S$ and $H_2$, is both reducing agent and sulfuring agent, the overall reaction equation is

$$2MoO_3 + 7S \rightarrow 2MoS_2 + 3SO_2 \quad (3)$$

Notwithstanding exact formation mechanism of synthesizing *IF*-$MoS_2$ nanoparticles using $MoO_3$ and S sublimations is still unclear, the synthesis method is contrasted with the reaction of $MoO_3$ and $H_2S$ in $H_2$ atmosphere, synthesized products are also including $MoO_2$, considering the literature[4,24,26,32] and experiment results, we infer the formation of *IF*-$MoS_2$ nanoparticles synthesized reacting the $MoO_3$ vapour with $H_2S$ is also the result of reduction and sulfuration. Possible reaction equations can be described as follows

$$MoO_3 + (x/2)\ S \rightarrow MoO_{3-x} + (x/2)\ SO_2 \quad (4)$$

$$MoO_{3-x} + (7 - x)/2\ S \rightarrow MoS_2 + (3 - x)/2\ SO_2 \quad (5)$$

where $0.1 < x < 0.5$. In the process of synthesis, $MoO_3$ precursors and S vapour are reactants. At lower temperature, incomplete reaction takes place and leads to forming an intermediate product due to the lower the activity of reactants. $MoO_2$ is one of the most stable in Mo compounds, so intermediate product exists generally in form of $MoO_2$. Below 750 °C, we obtained products including $MoO_2$. In Equation (4), if $x = 1$, the product becomes $MoO_2$, reaction equation is shown as

$$MoO_3 + (½)\ S \rightarrow MoO_2 + (½)\ SO_2 \quad (6)$$

## 4. Conclusion

By using $MoO_3$ and S (sulfur) as raw materials, $MoS_2$ nanoparticles with inorganic fullerene-like structure were reproducibly obtained by a chemical vapour deposition method as experiment conditions were precisely controlled. Highly pure Ar (argon) gas served as carrier gas in the synthesis process. This method broke though the limitation that corrosive toxic gas $H_2S$ or high-priced $H_2$ was unavoidable in the formation of *IF*-$MoS_2$ nanoparticles and nanotubes. On the basis of previous work and experimental results, a new reaction mode (formation mechanism) has been proposed, which method provides a scale-up and low-cost route to synthesizing *IF*-$MoS_2$ nanoparticles, laying foundations for further investigation of physical and chemical properties of the *IF*-$MoS_2$ raw materials. The synthetic approach can be potentially developed into a general method to preparing transition metal chalcogenides with the fullerene-like structure.

## Acknowledgements

This work was supported by the National Nature Science Foundation (51172187), the SPDRF and 111 Program (B08040) of MOE of China, the Special Scientific Research project Foundation of the Education Department of Shaanxi Province of China (09JK447), the special foundation item of the key academic subjects development of Shaanxi province [Shaanxi education Supporting (2008)169].

## References

1 H.W. Kroto, J.R. Heath, S.C. O'Brien, R. F. Crul and R.E. Smalley, *Nature*, 1985, 3**18**, 162–164.
2 S. Iijima, *Nature*, 1991, **354**, 56–58.
3 R. Tenne, L. Margulis, M. Genut and G. Hodes, *Nature*,1992, **360**, 444–446.
4 Y. Feldman, E. Wasserman, D.J. Srolovitz and R.Tenne, *Science*, 1995, **267**, 222–225.
5 M. Alaei, A. Rashidi and A. Mahjoub, *Iran. J. Chem. Chem. Eng.*, 2009, **28**, 91–95.
6 H.H. Wu, R. Yang, B.M. Song, Q.S. Han, J.Y. Li, Y. Zhang, Y. Fang, R. Tenne and C. Wang, *ACS Nano*, 2011, **5**, 1276–1291.
7 R. Tenne, M. Remskar, A. Enyashin and G. Seifert, *Topics Appl. Physics*, 2008, **111**, 631–672.
8 L. Rapoport, Yu. Bilik, Y. Feldman, M. Homyonfer, S.R. Cohen, R. Tenne and J. Israelachvily, *Nature*, 1997, **387**, 791–793.
9 L. Rapoport, N. Fleischer and R. Tenne, *J. Mater. Chem.*, 2005, **15**, 1782–1788.
10 J.J. Hu and J.S. Zabinski, *Tribol. Lett.*, 2005, **18**, 173–180.
11 Y.Q. Zhu, T. Sekine, Y.H. Li, M.W. Fay, Y.M. Zhao, C.H.P. Poa, W.X. Wang, R. Martin, P.D. Brown, N. Fleischer and R. Tenne, *J. Am. Chem. Soc.*, 2005, **127**, 16263–16272.
12 A. Kis, D. Mihailovic, M. Remskar, A. Mrzel, A. Jesih, I. Piwonski, A.J. Kulik, W. Benoit and L. Forro, *Adv. Mater.*, 2003, **15**, 733–735.
13 R. Dominko, M. Gaberscek, D. Arcon, A. Mrzel, M. Remskar, D. Mihailovic, S. Pejovnik and J. Jamnik, *Electrochim. Acta*, 2003, **48**, 3079–3084.
14 J. Chen, S.L. Li and Z.L. Tao, *J. Alloys Compd.*, 2003, **356**, 413–417.
15 H. Friedman, O. Eidelman, Y. Feldman, A. Moshkovich, V. Perfiliev, L. Rapoport, H. Cohen, A. Yoffe and R. Tenne, *Nanotechnology*, 2007, **18**, 115703–115711.
16 I. Kaplan-Ashiri, S.R. Cohen, K. Gartsman, V. Ivanovskaya, T. Heine, G. Seifert, I. Kanevsky, H.D. Wagner and R. Tenne, *Proc. Natl. Acad. Sci.*, 2006, **103**, 523–528.
17 J. Chen, S.L. Li, Q. Xu and K.J. Tanaka, *Chem. Commun.*, 2002, **16**, 1722–1723.
18 S.T. Wang, C.H. An and J.K. Yuan, *Materials*, 2010, **3**, 401–403.
19 P. A. Parilla, A.C. Dillon, K.M. Jones, G. Riker, D.L. Schulz, D.S. Ginley and M.J. Heben, *Nature,* 1999, **397**, 114–114.
20 J. Tannous, F. Dassenoy, I. Lahouij, T.L. Mogne, B. Vacher, A. Bruhács and W. Tremel, *Tribol. Lett.*, 2011, **41**, 55–64.
21 A.N. Enyashin, S. Gemming, M. Bar-Sadan, R. Popovitz-Biro, S.Y. Hong, Y. Prior, R. Tenne and G. Seifert, Angew. *Chem. Int. Ed. Engl.*, 2007, **46**, 623–627.
22 W.K. Hsu, B.H. Chang, Y.Q. Zhu, W.Q. Han, H. Terrones, M. Terrones, N. Grobert, A.K. Cheetham, H.W. Kroto and D.R.M. Walton, *J. Am. Chem. Soc.*, 2000, **122**, 10155–10158.

23 N. Sano, H.L. Wang, M. Chhowalla, I. Alexandrou, G.A.J. Amaratunga, M. Naito and T. Kanki, *Chem. Phys. Lett*., 2003, **368**, 331–337.

24 Y. Feldman, G.L. Frey, M. Homyonfer, V. Lyakhovitskaya, L. Margulis, H. Cohen, G.Hodes, J.L. Hutchison and R. Tenne, *J. Am. Chem. Soc*., 1996, **118**, 5362–5367.

25 Y. Feldman, V. Lyakhovitskaya and R. Tenne, *J. Am. Chem. Soc*., 1998, **120**, 4176–4183.

26 R.L.D. Whitby, W.K. Hsu, P.K. Fearon, N.C. Billingham, I. Maurin, H.W. Kroto, D.R.M. Walton, C.B. Boothroyd, S. Firth, R.J.H. Clark and D. Collison, *Chem. Mater.*, 2002, **14**, 2209–2217.

27 A. Margolin, R. Rosentsveig, A. Albu-Yaron, R. Popovitz-Biroand and R. Tenne, *J. Mater. Chem*., 2004, **14**, 617–624.

28 Y. Feldman, A. Zak, R. Popovitz-Biro and R. Tenne, *Solid State Sci.*, 2000, **2**, 663–672.

29 A. Zak, Y. Feldman, V. Alperovich, R. Rosentsveig and R. Tenne, *J. Am. Chem. Soc.*, 2000, **122**, 11108–11116.

30 G.L. Frey, A. Rothschild, J. Sloan, R. Rosentsveig, R. Popovitz-Biro and R. Tenne, *J. Solid State Chem*., 2001, **162**, 300–314.

31 G.L. Frey, R. Tenne, M.J. Matthews, M.S. Dresselhaus and G. Dresselhaus, *Phys. Rev. B*, 1999, **60**, 2883–2892.

32 R. Rosentsveig, A. Margolin, A. Gorodnev, R. Popovitz-Biro, Feldman, Y. L. Rapoport, G. Naveh and R. Tenne, *J. Mater. Chem*., 2009, **19**, 4368–4374.